

# Tapering Control of Si Nanowires Grown from SiCl<sub>4</sub> at Reduced Pressure

Sergiy Krylyuk,<sup>†</sup> Albert V. Davydov,<sup>†,\*</sup> and Igor Levin<sup>‡</sup>

<sup>†</sup>Metallurgy Division and <sup>‡</sup>Ceramics Division, Material Science and Engineering Laboratory, National Institute of Standards and Technology, Gaithersburg, Maryland 20899, United States

**ABSTRACT** Device applications of tapered Si nanowire (SiNW) arrays require reliable technological approaches for fabricating nanowires with controlled shape and orientation. In this study, we systematically explore effects of growth conditions on tapering of Si nanowires grown by chemical vapor deposition (CVD) at reduced pressure from SiCl<sub>4</sub> precursor. Tapering of SiNWs is governed by the interplay between the catalyzed vapor–liquid–solid (VLS) and uncatalyzed vapor–solid (VS) growth mechanisms. We found that the uncatalyzed Si deposition on NW sidewalls, defined by a radial growth rate, can be enhanced by lowering SiCl<sub>4</sub>/H<sub>2</sub> molar ratio, applying higher gas flow rate, or reducing growth pressure. Distinct dependences of the axial and radial growth rates on the process conditions were employed to produce SiNWs with a tapering degree (*i.e.*, a ratio of the radial/axial growth rates) varying by almost 2 orders of magnitude. The results are explained by an interplay between the thermodynamic and kinetic effects on the axial (VLS) and radial (VS) growth rates. Established correlation between the SiCl<sub>4</sub>/H<sub>2</sub> molar ratio and vertical alignment of nanowires was used to develop a two-stage growth procedure for producing tapered SiNW arrays with a predominantly vertical orientation.

**KEYWORDS:** silicon nanowires · tapering · vertical alignment

Tapered silicon nanowires (SiNWs) are prospective candidates for applications including field emitters,<sup>1–3</sup> electromagnetic sensors,<sup>4</sup> and nanomanipulators.<sup>5,6</sup> In particular, superior field-emission characteristics of tapered as compared to nontapered SiNWs have been reported.<sup>2</sup> Similarly to carbon nanocones,<sup>7</sup> conically shaped SiNWs are expected to exhibit higher bending stiffness than their prismatic counterparts. Unusual electronic properties of small diameter tapered SiNWs have been recently predicted.<sup>8</sup> Due to enhanced light absorption, vertically aligned arrays of tapered SiNWs are very promising for photovoltaic applications.<sup>9</sup> However, reliable technological approaches for fabricating SiNW arrays with controlled alignment and tapering have yet to be developed.

Broadly speaking, two strategies are being pursued to produce tapered SiNWs *via* the vapor–liquid–solid (VLS) mechanism: gradual volume reduction of the metal catalyst volume during the SiNW growth due

to diffusion, evaporation, or chemical reactions<sup>10,11</sup> and uncatalyzed vapor–solid (VS) Si deposition on the NW sidewalls while the catalytic droplet volume remains constant.<sup>12–16</sup> A shortcoming of the former approach is that the VLS growth eventually terminates when the catalyst droplet is consumed. The latter approach enables fabrication of SiNWs of an arbitrary length, with their tapering degree tuned by adjusting uncatalyzed *versus* catalyzed Si deposition rates. A combination of these two approaches also seems possible.<sup>17</sup>

In most cases, tapered SiNWs have been produced using silane-based CVD technique<sup>13,14,17</sup> because the relatively low decomposition temperature of SiH<sub>4</sub> favors film deposition on NW sidewalls. This approach, however, has several drawbacks. For example, change of growth conditions to increase the sidewall Si deposition rate also accelerates the vertical growth of the SiNWs, so that production of SiNWs of the same length but with different taper is difficult to achieve, conformally deposited Si shell can be amorphous or polycrystalline, and deposition of an undesirable Si layer on the substrate is difficult to avoid. It is also difficult to realize vertical alignment of SiNWs using SiH<sub>4</sub>. In contrast, the silicon tetrachloride (SiCl<sub>4</sub>) precursor permits silicon growth on the SiO<sub>2</sub>-covered Si surface to be easily suppressed<sup>18</sup> while, as noticed by Wagner and Ellis,<sup>19</sup> contamination-free sidewalls of SiNWs provide a perfect place for the epitaxial overgrowth even at conditions when single crystalline films cannot be obtained on planar Si substrates. Furthermore, the silicon deposition rate can be fine-tuned simply by varying the SiCl<sub>4</sub>/H<sub>2</sub> ratio.<sup>20</sup> Fabrication of vertically aligned silicon nano- and microwires using SiCl<sub>4</sub> pre-

\*Address correspondence to albert.davydov@nist.gov.

Received for review September 27, 2010 and accepted December 6, 2010.

Published online December 15, 2010. 10.1021/nn102556s

This article not subject to U.S. Copyright. Published 2011 by the American Chemical Society.

cursor has been recently demonstrated.<sup>21,22</sup> However, technological approaches to produce SiNWs with a controlled degree of taper remain largely unrealized.

Tapering of Al-, Ga-, and In-catalyzed SiNWs has been ascribed to a gradual decrease of the catalytic droplet diameter due to its incorporation into Si lattice and/or due to etching by hydrogen chloride, a byproduct of hydrogen reduction of SiCl<sub>4</sub>.<sup>11,23</sup> Garnett *et al.* found that, besides the growth temperature, tapering of Pt-catalyzed SiNWs can be reduced by lowering SiCl<sub>4</sub> partial pressure and total gas flow rate.<sup>24</sup> Givargizov described the tapering of Pt-catalyzed Si whiskers by introducing the “liquid phase effectivity coefficient” defined as the ratio of the axial to radial growth rates (GR),  $R_{ax}/R_{rad}$ .<sup>12</sup> He showed that this ratio decreases with temperature, mainly due to an increase of  $R_{rad}$ , and increases for higher SiCl<sub>4</sub> molar fractions due to an increase of  $R_{ax}$  at relatively constant  $R_{rad}$ . The results of refs 12 and 24 indicate that the tapering degree of SiCl<sub>4</sub>-grown SiNWs is governed by the interplay between the VLS and VS mechanisms. Therefore, establishment of the growth regimes that enhance/suppress one of these pathways of Si deposition is essential for producing SiNWs with a controllable tapered morphology.

This paper is focused on practical aspects of CVD growth of tapered SiNWs from the silicon tetrachloride (SiCl<sub>4</sub>) precursor. We have systematically studied the influence of the growth parameters, such as molar fractions of SiCl<sub>4</sub> ( $x_{SiCl_4}$ ) and H<sub>2</sub> ( $x_{H_2}$ ) in a SiCl<sub>4</sub>/H<sub>2</sub>/N<sub>2</sub> mixture, total gas flow rate, and reactor pressure on the growth kinetics and tapering of SiNWs produced at 850 °C; results for other growth temperatures are also briefly discussed. We show that, by varying the processing conditions, the tapering degree, which corresponds to the ratio of uncatalyzed to catalyzed Si deposition rates, can be varied by almost 2 orders of magnitude, thereby enabling fabrication of cone-shaped SiNWs with different apex angles. On the basis of the established correlation between the SiCl<sub>4</sub>/H<sub>2</sub> molar ratio and vertical NW alignment, a two-stage growth procedure for producing tapered SiNW arrays with predominantly vertical orientations is proposed. In contrast to earlier studies limited to ambient pressure,<sup>11,12,19,21–26</sup> we report on growth of SiNWs from SiCl<sub>4</sub> at reduced pressure. Reduced-pressure CVD using a SiCl<sub>4</sub>/H<sub>2</sub> system offers benefits, including reduction of residual oxygen backpressure, which severely affects SiNWs growth,<sup>27</sup> possibility of obtaining superior quality single-crystalline Si films at lower temperatures,<sup>28</sup> *etc.* In this study, we found that lowering the growth pressure also enhances the radial growth of SiNWs, which can be utilized for fabrication of epitaxial core/shell SiNW structures.

## RESULTS AND DISCUSSION

**Effects of SiCl<sub>4</sub>/H<sub>2</sub> Ratio.** The SiNWs described here were grown at 850 °C and a total pressure  $P = 80$  kPa (600 Torr). SiCl<sub>4</sub> and H<sub>2</sub> flows were varied to maintain a de-

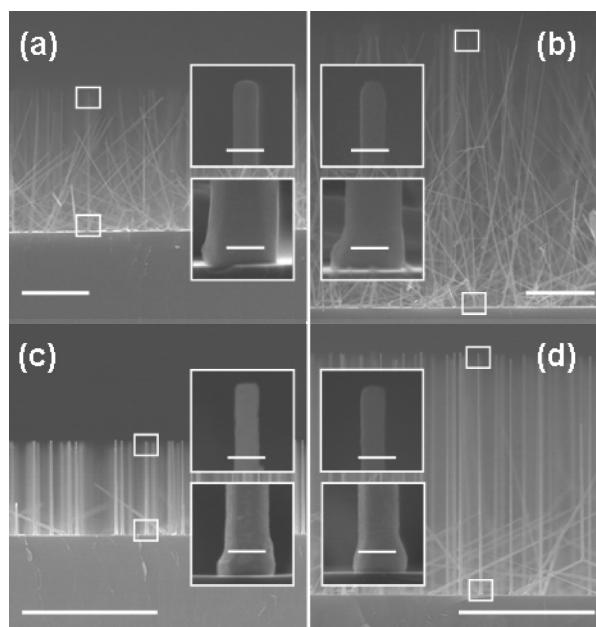


**Figure 1.** Cross-sectional SEM images of SiNWs grown for 5 min at SiCl<sub>4</sub>/H<sub>2</sub> ratio of (a,b) 0.03 and (c,d) 0.1. SiCl<sub>4</sub>/H<sub>2</sub> flow rates (in sccm) were (a) 5/168, (b) 15/500, (c) 5/50, and (d) 15/150; the total SiCl<sub>4</sub>/H<sub>2</sub>/N<sub>2</sub> flow was fixed at 1000 sccm. Scale bars are 10  $\mu$ m. Insets: bases and tips of SiNWs boxed in the main images. Scale bars are 200 nm.

sired SiCl<sub>4</sub>/H<sub>2</sub> ratio, and the diluent nitrogen flow was adjusted to keep the total gas flow rate ( $F$ ) at 1000 sccm (standard cm<sup>3</sup>/min). (Hereafter, the total gas flow rate refers to the direct SiCl<sub>4</sub>/H<sub>2</sub>/N<sub>2</sub> flow that delivers precursors into the reactor; the ratio of the direct-to-counter flows was kept at unity; see Experimental Section for details). Figure 1 shows cross-sectional SEM images of SiNWs grown for 5 min at SiCl<sub>4</sub>/H<sub>2</sub> = 0.03 and 0.1 using 5 and 15 sccm of SiCl<sub>4</sub>, respectively. Representative SEM images showing the tapered morphology of SiNWs are given in the insets.

In most cases, Au catalytic droplets are not observed at the tips of SiNWs; instead, traces of gold are found on the NW sidewalls (as discussed later, Figure 5). However, the average diameter of the NW tips ( $d_t$ ) remained constant throughout all experiments reported here ( $\langle d_t \rangle = 130 \pm 10$  nm), slightly larger than the diameter of the Au nanoparticles used to catalyze the growth. The length ( $L$ ) and the base diameter ( $d_b$ ) of the SiNWs increased linearly with the growth time, while  $d_t$  was essentially time-independent (Figure S1 of the Supporting Information). The slopes of the  $L(t)$  and  $d_b(t)$  dependences plotted in Figure S1 correspond to the axial and radial GRs, respectively. These findings imply that loss of the catalyst during growth, which could have contributed to the tapered morphology of SiNWs, is negligible; therefore, the observed NW tapering is caused by silicon deposition on the NW sidewalls. Migration of Au from the NW caps to the sidewalls after the growth completion will be discussed later.

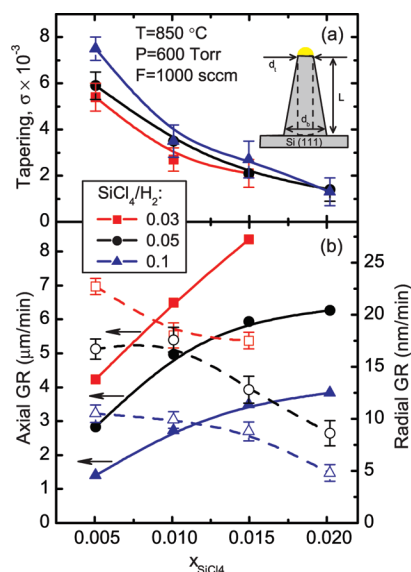


**Figure 2.** (a) Tapering degree  $\sigma$  and (b) axial (solid symbols) and radial (open symbols) GRs as a function of  $\text{SiCl}_4$  molar fraction for SiNWs grown at constant  $\text{SiCl}_4/\text{H}_2$  ratios as indicated. Hereafter, error bars represent the standard deviation of the measured values; errors bars for the axial GR are approximately equal to or less than the symbol size and omitted for clarity; lines are intended only to guide the eye. Inset in (a) schematically shows NW dimensions used to calculate the tapering degree.

The length and the base diameter of SiNWs grown at a fixed  $x_{\text{SiCl}_4}$  are proportional to the  $\text{H}_2$  molar fraction (*cf.*, images a–c and b–d in Figure 1). Simultaneous increase of  $x_{\text{SiCl}_4}$  and  $x_{\text{H}_2}$  at a fixed  $\text{SiCl}_4/\text{H}_2$  ratio leads to higher axial GRs, but the base diameters of SiNWs become smaller, which implies slower radial growth (*cf.*, images a,b and c,d in Figure 1).

These findings are further analyzed in Figure 2. The tapering degree of SiNWs, defined as  $\sigma = (d_b - d_t)/2L$  (refs 14 and 16) was calculated using NW dimensions determined from SEM images (inset in Figure 2a). TEM measurements on selected samples confirmed the SEM findings. The base diameters were measured at about 200–400 nm above the substrate level, with the correction for the length, in order to exclude “swelling” of the SiNWs’ base at the interface with the substrate that typically occurs during the initial stage of the growth.<sup>19</sup> Figure 2a shows the tapering degree as a function of  $\text{SiCl}_4$  concentration for  $\text{SiCl}_4/\text{H}_2 = 0.03, 0.05,$  and  $0.1$ . The trend is similar for all  $\text{SiCl}_4/\text{H}_2$  ratios, showing significantly reduced tapering for higher  $\text{SiCl}_4/\text{H}_2$  molar fractions. Similar behavior of the tapering was also observed for growth temperatures of 800 and 900 °C (Figure S2). Since the conical shape of SiNWs is caused by epitaxial Si deposition on the sidewalls, the tapering degree corresponds to the ratio of radial to axial growth rates,  $\sigma = R_{\text{rad}}/R_{\text{ax}}$ . Dependences of the axial and radial GRs on  $x_{\text{SiCl}_4}$  are plotted in Figure 2b. The radial GRs were calculated using the taper data from Figure 2a and the axial GRs determined from the SEM images.<sup>29</sup>

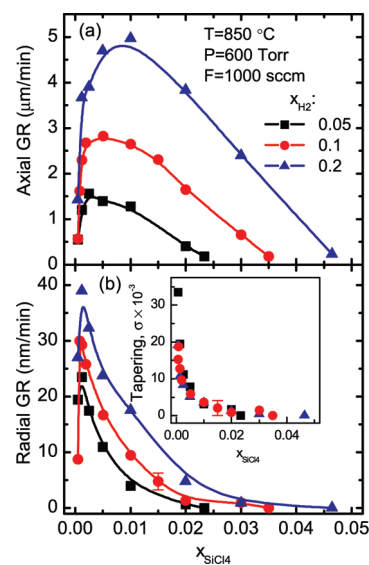


**Figure 3.** (a) Axial and (b) radial growth rates of SiNWs as a function of the  $\text{SiCl}_4$  molar concentration at three constant hydrogen molar fractions,  $x_{\text{H}_2}$ , as indicated. The error bars apply to all data in (b) and the inset, respectively. Inset: dependence of the tapering degree on  $x_{\text{SiCl}_4}$ .

For a constant  $x_{\text{SiCl}_4}$ , higher  $R_{\text{ax}}$  and  $R_{\text{rad}}$  are achieved for higher  $\text{H}_2$  molar fractions which can be attributed to more effective reduction of  $\text{SiCl}_4$  by hydrogen.<sup>30</sup> Increase of  $x_{\text{SiCl}_4}$  at constant ratio  $\text{SiCl}_4/\text{H}_2$  yields larger axial GRs, in agreement with the earlier reports on SiNWs growth from  $\text{SiCl}_4$  and  $\text{SiH}_4$ .<sup>12,13,24,31</sup> Significantly, as shown in Figure 2b, this is accompanied by a decrease of the radial GR. The axial and radial GRs can thus be tuned to produce SiNWs with different taper angles. As shown in Figure 2, the tapering degree varies by almost an order of magnitude. Below, we show that even larger tapering can be achieved when other growth conditions are altered.

**Effects of  $\text{SiCl}_4$  and  $\text{H}_2$  Molar Fractions.** In order to further explore control of the SiNWs tapering, detailed studies of the influence of  $\text{SiCl}_4$  and  $\text{H}_2$  molar fractions on the axial and radial growth of SiNWs were performed. In the commonly used  $\text{SiCl}_4/\text{H}_2$  system, it is difficult to separate the effects of the two species because adding more  $\text{SiCl}_4$  automatically reduces the molar fraction of hydrogen for constant flow rate. Inert gas dilution enables independent variation of  $x_{\text{SiCl}_4}$  and  $x_{\text{H}_2}$  for given flow rate, enabling systematic study and control of the effects of the two precursors.

Figure 3 shows the axial and radial GRs of SiNWs as a function of the  $\text{SiCl}_4$  molar fraction for  $x_{\text{H}_2} = 0.05, 0.1,$  and  $0.2$ . The tapering degree *versus*  $x_{\text{SiCl}_4}$  is plotted in the inset in Figure 3. The GR trends qualitatively resemble those obtained for  $\text{SiCl}_4$ -grown thin films.<sup>20,30</sup> The radial GR rapidly increases with increasing  $x_{\text{SiCl}_4}$  reaching a maximum at  $x_{\text{SiCl}_4} \approx 0.0012$  and then decreases with exponential-like behavior. The initial increase of the axial GR is slower, and in general, higher  $\text{SiCl}_4$  concentrations are needed to achieve a maximum axial GR. Ex-

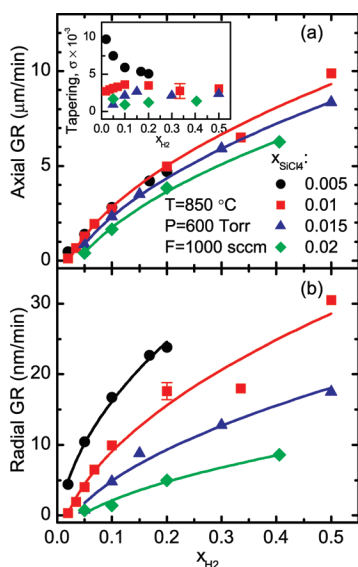


**Figure 4.** (a) Axial and (b) radial growth rates as a function of the hydrogen molar fraction at constant  $\text{SiCl}_4$  molar fractions,  $x_{\text{SiCl}_4}$ , as indicated. The lines are  $R_{\text{ax(rad)}} \sim x_{\text{H}_2}^{1/2}$  fits. The error bars apply to all data in (b) and the inset, respectively. Inset: dependence of the tapering degree on  $x_{\text{H}_2}$ .

trapolation of the axial GR dependences to zero indicates that, for these particular experimental conditions, VLS growth of SiNWs does not proceed if  $x_{\text{SiCl}_4}$  exceeds  $\approx 0.025$ ,  $\approx 0.036$ , and  $\approx 0.047$  for  $x_{\text{H}_2} = 0.05$ ,  $0.1$ , and  $0.2$ , respectively; control experiments at  $x_{\text{SiCl}_4} = 0.03$  and  $x_{\text{H}_2} = 0.05$  produced triangular etch pits around the Au nanoparticles with no NWs. Note that, for our experimental conditions, sustainable growth of straight SiNWs could be achieved only for  $x_{\text{SiCl}_4} \geq 0.0025$ . Although SiNWs grown at lower  $\text{SiCl}_4$  fractions exhibited the largest tapering, most of them were severely bent and kinked, which precludes their use for device applications.

Experiments performed at the same conditions as above but at fixed  $\text{SiCl}_4$  concentrations (Figure 4) showed that the axial and radial GRs both increase with the hydrogen partial pressure, as expected. In contrast to the radial GR, no appreciable variation in the axial GR is observed for  $x_{\text{SiCl}_4}$  below *ca.* 0.01. The tapering degree (inset in Figure 4a) is only weakly dependent on the hydrogen content for  $x_{\text{SiCl}_4} \geq 0.01$ , indicating that both  $R_{\text{ax}}$  and  $R_{\text{rad}}$  scale similarly with  $x_{\text{H}_2}$ ; for lower  $\text{SiCl}_4$  concentrations, the tapering degree decreases with  $x_{\text{H}_2}$ . Both GRs can be fitted by  $R_{\text{ax(rad)}} \sim x_{\text{H}_2}^{1/2}$  (lines in Figure 4). The origin of this dependence is unclear, especially in light of the different mechanisms involved in the Si deposition on the sidewalls and through the catalytic liquid droplets.

The notably distinct dependences of the axial and lateral GRs on the  $\text{SiCl}_4$  and  $\text{H}_2$  concentrations enable fabrication of SiNWs having similar length but different degree of tapering. For example, the axial GRs of SiNWs grown at  $x_{\text{SiCl}_4} \approx 0.02$  and  $\approx 0.001$  (at fixed  $x_{\text{H}_2} = 0.1$ , Figure 3) are about the same ( $\approx 1.6$   $\mu\text{m}/\text{min}$ ), whereas the

radial GRs are  $\approx 1.4$  and  $\approx 30$   $\text{nm}/\text{min}$ , respectively, yielding about a 20-fold increase of the tapering degree.

**Structural Studies.** As noted earlier, tapered SiNWs produced at  $x_{\text{SiCl}_4} < 0.0025$  exhibited a very high density of structural defects, indicating a trade-off between high radial growth rates and structural perfection of the epitaxial shell. The crystallographic quality of SiNWs grown at higher  $\text{SiCl}_4$  concentrations is significantly improved. Panels a and b of Figure 5 show representative TEM images of SiNWs grown at  $x_{\text{H}_2} = 0.1$  and  $x_{\text{SiCl}_4} = 0.005$  and  $0.03$ , respectively.

The  $\text{SiCl}_4/\text{H}_2$  ratio also affects Au migration out of the SiNW tip. As seen in Figure 5a, the Au catalyst completely disappears from the NW tips and tiny gold droplets reside on the NW side facets (middle inset in Figure 5a). In contrast, Au droplets, although severely deformed, still stay atop SiNWs grown at higher  $\text{SiCl}_4$  molar fractions, as shown in Figure 5b. Oehler *et al.*<sup>32</sup> recently reported that absorption of Cl atoms on the SiNW sidewalls significantly reduces the Au loss from the Au–Si catalytic droplet. Thus, the difference between panels a and b in Figure 5 could be attributed to a higher Cl coverage of the NW sidewalls shown in Figure 5b. In agreement with recent reports,<sup>26,33</sup> our experiments also confirmed that gold migration off the NW tips occurs during the cool-off stage. Since Au impurities act as deep-level traps in silicon and it is difficult to completely remove Au from SiNW stems by wet etching,<sup>34</sup> the postgrowth Au migration should be minimized. We found that Au droplets can be preserved at the NW tips by fast cooling of the samples from the growth temperature down to  $\approx 500$   $^\circ\text{C}$  in about 10 s (Figure S3). We also noticed that more catalyst material stayed atop SiNWs having larger diameters (see Figure S4).

**Effects of Total Gas Flow Rate and Growth Pressure.** In the previous sections, we showed that lowering the  $\text{SiCl}_4$  partial pressure favors growth of SiNWs with significant tapering. In those experiments, both the growth pressure and the  $\text{SiCl}_4/\text{H}_2/\text{N}_2$  input flow rate were fixed at 600 Torr and 1000 sccm, respectively, thus maintaining invariant gas flow conditions in the reactor. Here, we explore how these parameters affect the growth of SiNWs.

Tapering degree as well as the axial and radial GRs of SiNWs grown at different  $\text{SiCl}_4/\text{H}_2/\text{N}_2$  input flow rates are plotted in Figure 6. The experiments were conducted at  $T = 850$   $^\circ\text{C}$ ,  $P = 600$  Torr, and  $\text{SiCl}_4/\text{H}_2 = 0.1$ . The radial GR of SiNWs grown at a fixed  $x_{\text{SiCl}_4}$  roughly scaled with the total flow rate in the range of the  $\text{SiCl}_4$  molar fractions used (Figure 6b). GR increase with the total flow has also been reported for  $\text{SiCl}_4$ -grown thin films.<sup>20</sup> Garnett *et al.* also mentioned a reduced tapering of SiNWs grown at lower gas flow rates, although no details were presented.<sup>24</sup> Less distinct gas flow rate dependence is seen for the axial GR (Figure 6b). For example, very similar axial GRs (2.1 and 1.8  $\mu\text{m}/\text{min}$ ) were

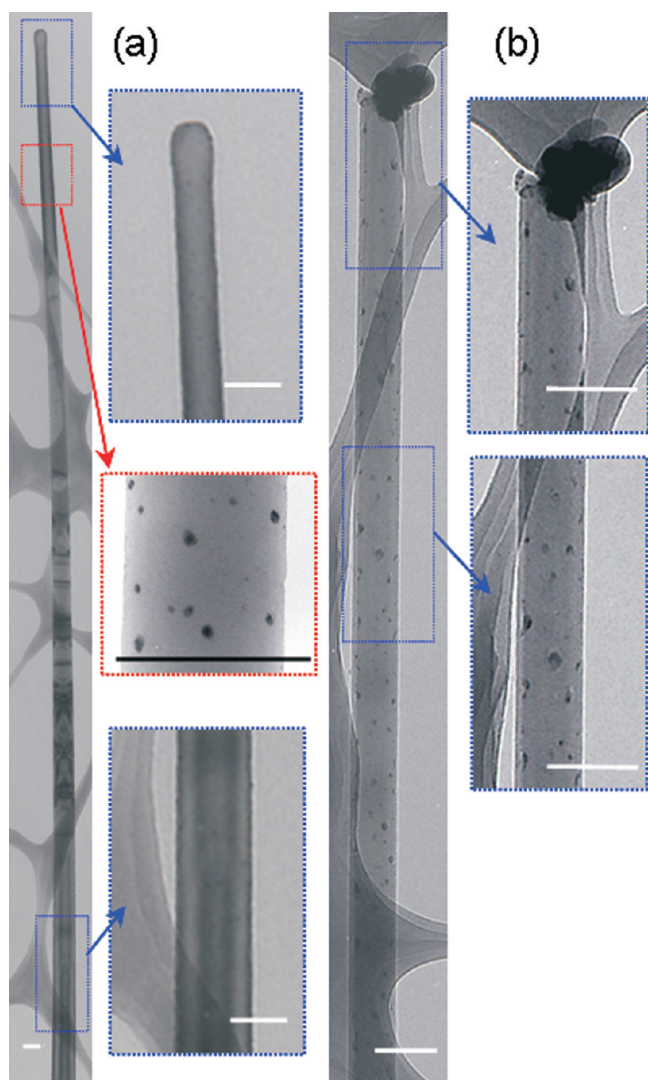


**Figure 5.** (a) TEM image of a 12  $\mu\text{m}$  long tapered SiNW grown at  $x_{\text{H}_2} = 0.1$  and  $x_{\text{SiCl}_4} = 0.005$ . Insets show a closer view of the different parts of the NW; Au droplets on the NW surface appear as dark spots in the middle inset; the contrast in the lower inset is due to thickness variation resulting from the hexagonal cross section of the NW. (b) TEM image a 3.3  $\mu\text{m}$  long SiNW grown at  $x_{\text{H}_2} = 0.1$  and  $x_{\text{SiCl}_4} = 0.03$ . For this NW, no significant tapering is observed. Most of the Au catalyst is visible at the NW's tip, with Au droplets again visible down the NW sidewalls. Scale bars are 200 nm.

obtained for SiNWs grown at  $x_{\text{SiCl}_4} = 0.0074$  and the total flow rate of 500 and 2000 sccm, while the respective radial GRs were about 5 and 19 nm/min. Corresponding SEM images are shown in Figure S5. For the highest  $x_{\text{SiCl}_4}$  values used,  $R_{\text{ax}}$  did increase with the total gas flow; however, its relative variation was still much smaller than that of the radial GR.

The distinct difference in the axial and radial GR dependences on the gas flow rate is intriguing. The increase of  $R_{\text{rad}}$  could be due to the fact that the larger mass input of the reactants is (which can be achieved by increasing total gas flow rate at fixed  $x_{\text{SiCl}_4}$  and  $x_{\text{H}_2}$ ), the more  $\text{SiCl}_4$  can be converted to solid silicon. Additionally,  $R_{\text{rad}}$  could increase due to the following effect:

as the thickness of the boundary layer decreases with the linear gas velocity increasing, diffusive flow of the reactants toward the Si surface is enhanced. On the other hand, it appears that these factors only weakly affect the axial GR, which for the present experiments is mainly determined by the partial pressure of  $\text{SiCl}_4$ , especially for low  $\text{SiCl}_4$  molar fractions. Although additional studies are required to understand this phenomenon, increasing the gas flow rate (at constant  $x_{\text{SiCl}_4}$  and  $x_{\text{H}_2}$ ) clearly enhances the tapering of SiNWs (Figure 6a).

Next, we study the influence of the reactor pressure on the growth kinetics of SiNWs. In this study, the  $\text{SiCl}_4/\text{H}_2/\text{N}_2$  flow rate was kept at 1000 sccm. Two series of experiments were conducted: (1) growth at constant mass inputs and (2) at constant partial pressures of the precursors. In the first case, the  $\text{SiCl}_4$  and  $\text{H}_2$  partial pressures,  $p_{\text{SiCl}_4}$  and  $p_{\text{H}_2}$ , scaled with the total pressure according to  $p_{\text{SiCl}_4(\text{H}_2)} = x_{\text{SiCl}_4(\text{H}_2)} \times P$ . The molar fractions used were  $x_{\text{SiCl}_4}/x_{\text{H}_2} = 0.01/0.2$ ,  $0.01/0.1$ , and  $0.02/0.1$ . At  $P = 600$  Torr, they yield the respective partial pressures  $p_{\text{SiCl}_4}/p_{\text{H}_2} = 6/120$ ,  $6/60$ , and  $12/60$  Torr. These partial pressures were fixed in the second series of experiments in which  $x_{\text{SiCl}_4}$  and  $x_{\text{H}_2}$  scaled similarly with the growth pressure.

As seen in Figure 7a, the axial GR of SiNWs grown at constant mass inputs increases with pressure, and except for the lowest growth pressures employed, lower  $\text{SiCl}_4/\text{H}_2$  ratios yielded higher  $R_{\text{ax}}$ . Similar behavior of  $R_{\text{ax}}$  was described earlier when partial pressures were lowered by  $x_{\text{SiCl}_4}/x_{\text{H}_2}$  reduction at  $P = 600$  Torr (see Figures 2 and 6). For a given  $\text{SiCl}_4/\text{H}_2$  ratio, varying the growth pressure while keeping  $p_{\text{SiCl}_4}$  and  $p_{\text{H}_2}$  constant did not cause appreciable changes of the axial GR over the whole explored range of 250–700 Torr (open symbols in Figure 7a). This confirms that for our experimental conditions the axial GR essentially depends on the  $\text{SiCl}_4$  and  $\text{H}_2$  partial pressures, which determine fluxes of the reactants impinging on the catalytic droplets.

Lowering the growth pressure at  $\text{SiCl}_4/\text{H}_2 = \text{constant}$  resulted in almost the same variation of the radial GRs, regardless of whether SiNWs were grown at constant mass input or constant partial pressure (Figure 7b). For  $P \leq 300$  Torr and  $\text{SiCl}_4/\text{H}_2 = 0.1$  and  $0.2$ , lower radial GRs of SiNWs grown at  $p_{\text{SiCl}_4}/p_{\text{H}_2} = \text{constant}$  (triangles and circles in Figure 7b) apparently reflect the situation observed in Figures 2 and 6 where  $R_{\text{rad}}$  decreased with increasing  $\text{SiCl}_4/\text{H}_2$  concentration. This difference vanishes for higher growth pressures as the precursor flows used in the two series of experiments become comparable. Moreover,  $R_{\text{rad}}$  values obtained for  $x_{\text{SiCl}_4}/x_{\text{H}_2} = 0.01/0.2$  and  $p_{\text{SiCl}_4}/p_{\text{H}_2} = 6/120$  are undistinguishable even at 250 Torr despite 2.4-fold increase in  $\text{SiCl}_4/\text{H}_2$  flow for the latter ( $x_{\text{SiCl}_4}/x_{\text{H}_2} = 0.024/0.48$ ). Tapering degrees obtained at 250 Torr were in the range of 0.028 to 0.05 (see Figure S6); that is,  $R_{\text{ax}}$  is only 20 to 35 times larger than  $R_{\text{rad}}$ , whereas for nominally untapered SiNWs,  $R_{\text{ax}}/R_{\text{rad}}$  is at least 1000.

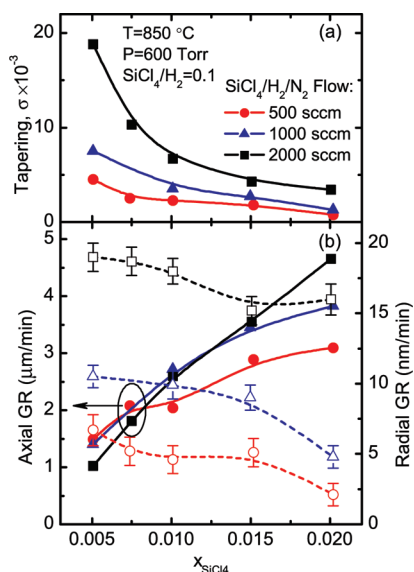


**Figure 6.** (a) Tapering degree and (b) axial (solid symbols) and radial (open symbols) growth rates as a function of  $\text{SiCl}_4$  molar fraction for SiNWs grown at 850 °C, 600 Torr,  $\text{SiCl}_4/\text{H}_2 = 0.1$ , and the total  $\text{SiCl}_4/\text{H}_2/\text{N}_2$  flow rate of 500, 1000, and 2000 sccm.

Compared to the above approaches of controlling SiNW shape, growth at low pressures enables fabrication of SiNWs with even larger tapering and superior structural quality. Using a proper combination of reactant concentrations, gas velocity, and growth pressure, the shape of SiNWs can be fine-tuned. An example is given in Figure 8, showing arrays of SiNWs with rod-like and cone-like shapes that were grown at 600 and 300 Torr using  $\text{SiCl}_4/\text{H}_2$  molar fractions of 0.03/0.2 and 0.01/0.1, respectively. In both cases, VLS growth was

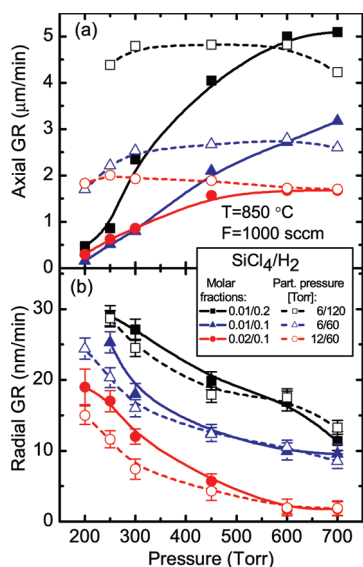


**Figure 7.** Dependences of (a) axial and (b) radial growth rates of SiNWs on the growth pressure. SiNWs were grown at constant mass inputs (solid symbols) or at constant partial pressures (open symbols) of  $\text{SiCl}_4$  and  $\text{H}_2$ , as indicated. Data from two different experiments at  $P = 600$  Torr are given in order to illustrate high reproducibility of the results.

catalyzed by 100 nm diameter Au dots patterned with e-beam lithography.

**Vertical Alignment of Tapered SiNWs.** For many device applications, arrays of SiNWs normal to a Si(111) substrate are required. However, low  $\text{SiCl}_4/\text{H}_2$  ratios, which facilitate the radial growth, negatively impact epitaxy of SiNWs with the underlying substrate; an increase in the  $\text{SiCl}_4/\text{H}_2$  ratio significantly improves vertical alignment of SiNWs but suppresses the tapering. This is illustrated in Figure 9a,b, showing SiNWs grown at  $x_{\text{H}_2} = 0.1$  and  $\text{SiCl}_4/\text{H}_2$  ratio of 0.05 and 0.3, respectively. For the latter, about 85% of SiNWs grew vertically (fraction of vertical SiNWs is the average of several  $\sim 50 \mu\text{m} \times 60 \mu\text{m}$  areas randomly selected on the substrate). Most of the SiNWs produced at  $\text{SiCl}_4/\text{H}_2 = 0.05$  were randomly oriented, although they still preserved a  $\langle 111 \rangle$  growth direction as confirmed by TEM. This demonstrates that SiNWs' epitaxy/alignment is very sensitive to the  $\text{SiCl}_4/\text{H}_2$  ratio which, as discussed below, defines the supersaturation: lower supersaturations achieved at higher  $\text{SiCl}_4/\text{H}_2$  ratios cause preferential growth of SiNWs along the [111] direction normal to the Si(111) surface. Ge *et al.*<sup>35</sup> suggested that effective supersaturation increases as less silicon is deposited on the reactor walls during successive depositions, and this eventually deteriorates SiNW alignment due to an increased probability of homogeneous nucleation. Our studies did not reveal any essential difference in alignment of SiNWs produced with or without parasitic Si deposition on reactor walls; the fraction of vertically growing SiNWs depended primarily on the  $\text{SiCl}_4/\text{H}_2$  ratio.

Using the established correlation between the  $\text{SiCl}_4/\text{H}_2$  ratio and the SiNWs alignment, a two-stage growth procedure was developed to produce vertically oriented arrays of tapered SiNWs. The growth was initiated at a high  $\text{SiCl}_4/\text{H}_2$  ratio (typically,  $\text{SiCl}_4/\text{H}_2 \geq 0.3$ ) to ensure good vertical alignment of SiNWs and, after 1 to 2 min, proceeded at a lower  $\text{SiCl}_4/\text{H}_2$  ratio achieved by either introducing more hydrogen to the system or decreasing the  $\text{SiCl}_4$  concentration. During the second stage, SiNWs regained the axial and radial GRs corresponding to the selected  $\text{SiCl}_4/\text{H}_2$  ratio but maintained the predominant vertical orientation from the first stage as shown in Figure 9c,d.

**Discussion.** Our results demonstrated that, due to high sensitivity of the axial and radial GRs to the processing conditions,  $\text{SiCl}_4$ -based reduced-pressure CVD offers flexibility in manipulating the shape of SiNWs. In this section, we briefly discuss some mechanisms that might be responsible for the observed dependences of  $R_{\text{ax}}$  and  $R_{\text{rad}}$ . In-depth understanding of the processes involved in catalyzed and uncatalyzed Si deposition from the Si–Cl–H–N system requires additional studies, such as studies of temperature dependence of  $R_{\text{ax}}$  and  $R_{\text{rad}}$  at different compositions of the  $\text{SiCl}_4/\text{H}_2/\text{N}_2$  gas mixture and growth pressures.

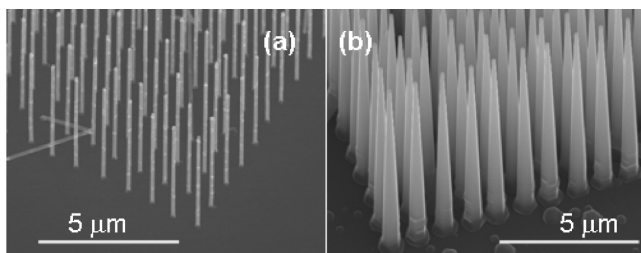
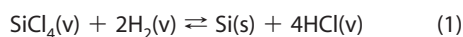


**Figure 8.** SEM images (30° tilt) of SiNWs produced at (a)  $x_{\text{SiCl}_4}/x_{\text{H}_2} = 0.03/0.2$  and 600 Torr for 5 min and (b)  $x_{\text{SiCl}_4}/x_{\text{H}_2} = 0.01/0.1$ , 300 Torr for 15 min. Arrays of Au dots (100 nm diameter, 75 nm thick) were fabricated using e-beam lithography.  $T = 850^\circ\text{C}$ ,  $F = 1000$  sccm.

The simplified thermodynamic description of silicon deposition can be expressed as



According to thermodynamic calculations for our typical growth conditions the dominant Si-containing gas species in the Si–Cl–H–N are  $\text{SiCl}_4$  (see Figure S7). Because of relatively low growth temperatures, Si deposition rate is determined by the kinetics of surface reactions either on SiNW sidewalls or, for the VLS growth, on the Au–Si liquid droplet. It has been shown for the kinetic regime that the rate-limiting step for reaction 1 is the reaction of  $\text{SiCl}_4$  with the surface silicon atoms:<sup>30</sup>

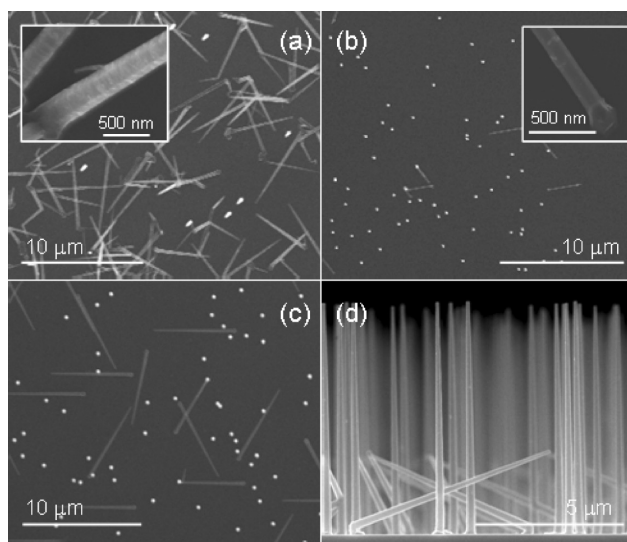
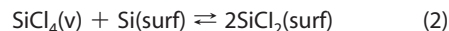
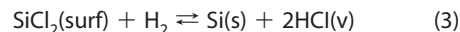


**Figure 9.** (a,b) Planview SEM images of SiNWs showing a negative correlation between vertical orientation and tapering for SiNWs grown for 5 min at a  $\text{SiCl}_4/\text{H}_2$  ratio of (a) 0.05 (tapered randomly oriented NWs) and (b) 0.3 (nontapered vertically oriented NWs, which appear as bright dots). (c) Plane- and (d) cross-sectional views of tapered SiNWs with improved vertical epitaxy produced by a two-stage growth procedure: growth started at  $\text{SiCl}_4/\text{H}_2 = 0.3$  and, after 1 min, proceeded at  $\text{SiCl}_4/\text{H}_2 = 0.05$ . For this particular experiment, the  $\text{SiCl}_4/\text{H}_2$  ratio was lowered by reducing the  $\text{SiCl}_4$  flow rate from 30 to 5 sccm, while keeping the  $\text{H}_2$  flow rate at 100 sccm.



Conceivably, similar reactions occur on the surface of the catalytic droplet giving rise to the VLS growth while silicon supply to the droplet *via* surface diffusion on the sidewalls is negligibly small. In this case, the axial GR of SiNWs would depend on the  $\text{SiCl}_4$  and  $\text{H}_2$  fluxes impinging on the Au–Si droplets, which are proportional to the respective partial pressures, and on the rate of reaction 3 determined by the  $\text{SiCl}_4/\text{H}_2$  ratio. Such dependence was confirmed in our experiments. For example, as shown in Figure 3a, the axial GR increases with  $x_{\text{SiCl}_4}$ , as long as sufficient hydrogen is available, and then saturates at  $\text{SiCl}_4/\text{H}_2 \approx 0.05$ . The subsequent decline of  $R_{\text{ax}}$  can be explained by retardation of reaction 3 and, correspondingly, increased probability of  $\text{SiCl}_2$  desorption from the surface. Extensive theoretical and experimental studies have indicated preferential removal of the surface Si atoms in the form of  $\text{SiCl}_2$ .<sup>36–38</sup> The feasibility of  $\text{SiCl}_4$  etching of SiNWs at  $850^\circ\text{C}$  was also confirmed in our experiments when the hydrogen flow was turned off after the growth and SiNWs were kept in the  $\text{SiCl}_4/\text{N}_2$  atmosphere (data not shown). For example, after a 5 min exposure to  $\text{SiCl}_4$ , the base diameters of SiNWs grown for 5 min at  $x_{\text{SiCl}_4}/x_{\text{H}_2} = 0.01/0.1$  shrank from *ca.* 228 to 160 nm. Liquid Au–Si droplets atop SiNWs enhanced the etching rate along the NW growth direction, in agreement with Wagner’s model of solid–liquid–vapor etching.<sup>39</sup>

From the thermodynamic viewpoint,<sup>40,41</sup> higher  $\text{SiCl}_4/\text{H}_2$  input ratios increase the solubility of silicon in the gas phase which in turn reduces supersaturation and ultimately causes Si etching *via* reaction 2. Moreover, for  $\text{SiCl}_4/\text{H}_2 = \text{constant}$ , supersaturation was shown to decrease when the total pressure of the reactants,  $p_{\text{SiCl}_4} + p_{\text{H}_2}$ , is increased.<sup>41</sup> This might be responsible for the more gradual increase of the axial GR observed for  $x_{\text{SiCl}_4} \geq 0.015$  (Figures 2b and 6b); an alternative explanation related to saturation of the crystallization rate of Si atoms on the liquid–solid interface is also possible.<sup>42</sup>

The above arguments are also applicable to the radial GR behavior; however, additional factors presumably affecting the uncatalyzed Si deposition must be taken into account. First of all, the effective supersaturations over the liquid Au–Si droplet and over the SiNW facets can be different, which manifests in vastly different  $R_{\text{ax}}$  and  $R_{\text{rad}}$  values. Also, kinetically, the VLS growth is in practice not limited by the number of sites available for adsorption of the reactants due to a very high accommodation coefficient of the liquid surface for the Au–Si droplet.<sup>19</sup> On the contrary, most of the surface Si atoms can be passivated by adsorbed H, Cl, and  $\text{SiCl}_2$  species. According to Chernov,<sup>43,44</sup> the fraction of free sites is only about (1 to 1.5) % at  $\approx 1200^\circ\text{C}$ , and it is expected to be even lower at our growth temperatures due to a longer residence time of the adsorbed atoms/

molecules. The number of free sites depends on the rates of desorption and surface reaction of the adsorbed species, both of which are proportional to temperature, as well as on the adsorption rates proportional to partial pressures of gas species. Thus, increasing the  $\text{SiCl}_4/\text{H}_2$  supply might reduce the number of vacancies on the NW sidewalls, provided that surface reaction rates are not significantly affected. Therefore, it is plausible to assume that a decreased fraction of available free sites contributes to the observed retardation of the radial GR at  $\text{SiCl}_4/\text{H}_2 = \text{constant}$  (Figures 2b and 6b). Higher growth temperatures accelerate reaction/desorption processes on the surface and could lead to a different dependence of the radial GR on the precursor concentration, as, for example, shown in Figure S2 for SiNWs grown at  $T = 900^\circ\text{C}$ . This assumption is supported by the pressure dependence of the radial GR obtained at constant partial pressures of  $\text{SiCl}_4$  and  $\text{H}_2$  (open symbols in Figure 7b). In this case, weak variations of the radial GR might be expected, similarly to the observed  $R_{\text{ax}}$  dependences (open symbols in Figure 7a). However, lower growth pressures facilitate desorption from the NW surface (most importantly, the deposition-poisoning Cl atoms) leading to higher radial GRs.

## EXPERIMENTAL SECTION

The experiments were carried out in a reduced-pressure horizontal hot-wall CVD system comprising a 76 mm diameter quartz reactor inserted into a 4-zone clamshell split furnace. Design of the reactor, which includes a purge zone where substrates can be held at a desired temperature in an inert atmosphere maintained by the nitrogen counter flow, allows fast (within a few seconds) initiation/termination of the growth through motion of a quartz susceptor with substrates into and out of the growth zone. The movable susceptor also allows for rapid heating/cooling of the substrates. This design minimizes uncertainties related to NWs' growth during transients regimes, such as when precursor flows are switched on/off and hence their concentration varies with time, and also provides a useful means for growing NWs with modulated composition, doping level, etc. It was determined that, for a direct-to-counter flow ratio close to unity, the counter flow does not affect the gas composition in the growth zone while preventing access of precursors into the purge zone.

Growth of SiNWs was catalyzed by commercially available 100 nm Au nanoparticles which were cast on poly-L-lysine-functionalized p-Si(111) substrates with native oxide. SiNWs were grown at 800–900 °C and total reactor pressure of 250–700 Torr. The growth time varied between 3 and 15 min. The samples were first annealed for 5 min at the growth temperature in 10%  $\text{H}_2/\text{N}_2$  followed by a 2–3 min  $\text{N}_2$  annealing in the purge zone to stabilize gas flow after introducing  $\text{SiCl}_4$ .  $\text{SiCl}_4$  vapor was delivered by bubbling nitrogen carrier gas through a  $\text{SiCl}_4$  bubbler held at 10 °C and 780 Torr. Changes of  $\text{SiCl}_4$  and/or  $\text{H}_2$  flow rates were compensated with the nitrogen flow to keep the total direct gas flow rate of  $\text{SiCl}_4/\text{H}_2/\text{N}_2$  mixture constant. The ratio between the direct and counter flows was always unity. SiNW morphologies and microstructures were examined using SEM and TEM. The accuracy of measurements of SiNW diameters using SEM was estimated at  $\pm 6$  nm, which is about 5% of the minimal NW diameter.

**Acknowledgment.** We thank Dr. Jong-Yoon Ha (NIST) for fabrication of e-beam lithographed arrays of Au dots on Si substrate used for SiNWs growth.

## CONCLUSIONS

In conclusion, we systematically studied effects of the growth parameters on the tapering of Au-catalyzed SiNWs produced from diluted  $\text{SiCl}_4/\text{H}_2$  mixture at 850 °C and reduced pressure. Low  $\text{SiCl}_4/\text{H}_2$  input ratios, high linear gas velocities, and low growth pressures promote epitaxial silicon deposition on the SiNW sidewalls. For SiNWs grown at a constant  $\text{SiCl}_4/\text{H}_2$  ratio, decrease of the precursor concentration resulted in a higher radial GR whereas the axial GR decreased. By choosing a proper combination of the growth conditions, the tapering degree was varied by almost 2 orders of magnitude. Since the growth conditions yielding large tapering degrees deteriorate epitaxy and vertical alignment of SiNWs on Si(111) substrates, we proposed a two-stage growth procedure which significantly improves the vertical orientation of tapered SiNWs. The presented results enable well-controlled tuning of the SiNWs shape and should enable production of arrays of tapered SiNWs as well as epitaxial core/shell NW structures. These results should also be applicable to CVD growth of SiNWs using other chlorosilanes and  $\text{SiH}_4/\text{HCl}$  mixtures.

*Supporting Information Available:* Additional graphs and SEM images. This material is available free of charge via the Internet at <http://pubs.acs.org>.

## REFERENCES AND NOTES

- Bai, X. D.; Zhi, C. Y.; Liu, S.; Wang, E. G.; Wang, Z. L. High-Density Uniformly Aligned Silicon Nanotip Arrays and Their Enhanced Field Emission Characteristics. *Solid State Commun.* **2003**, *125*, 185–188.
- Chuen, Y. L.; Chou, L. J.; Hsu, C. M.; Kung, S. C. Synthesis and Characterization of Taper- and Rodlike Si Nanowires on  $\text{Si}_x\text{Ge}_{1-x}$  Substrate. *J. Phys. Chem. B* **2005**, *109*, 21831–21835.
- Fang, X.; Bando, Y.; Gautam, U. K.; Ye, C.; Golberg, D. Inorganic Semiconductor Nanostructures and Their Field-Emission Applications. *J. Mater. Chem.* **2008**, *18*, 509–522.
- Cao, L.; Nabet, B.; Spanier, J. E. Enhanced Raman Scattering from Individual Semiconductor Nanocones and Nanowires. *Phys. Rev. Lett.* **2006**, *96*, 157402.
- Hashiguchi, G.; Goda, T.; Hosogi, M.; Hirano, K.; Kaji, N.; Baba, Y.; Kakushima, K.; Fujita, H. DNA Manipulation and Retrieval from an Aqueous Solution with Micromachined Nanotweezers. *Anal. Chem.* **2003**, *75*, 4347–4350.
- Yamahata, C.; Collard, D.; Legrand, B.; Takekawa, T.; Kumemura, M.; Hashiguchi, G.; Fujita, H. Silicon Nanotweezers with Subnanometer Resolution for the Micromanipulation of Biomolecules. *J. Microelectromech. Syst.* **2008**, *17*, 623–631.
- Wei, C.; Srivastava, D. Nanomechanics of Carbon Nanofibers: Structural and Elastic Properties. *Appl. Phys. Lett.* **2004**, *85*, 2208.
- Wu, Z.; Neaton, J. B.; Grossman, J. C. Quantum Confinement and Electronic Properties of Tapered Silicon Nanowires. *Phys. Rev. Lett.* **2008**, *100*, 246804.
- Zhu, J.; Yu, Z.; Burkhard, G. F.; Hsu, C.-M.; Connor, S. T.; Xu, Y.; Wang, Q.; McGehee, M.; Fan, S.; Cui, Y. Optical Absorption Enhancement in Amorphous Silicon Nanowire and Nanocone Arrays. *Nano Lett.* **2009**, *9*, 279–282.

10. Hannon, J. B.; Kodambaka, S.; Ross, F. M.; Tromp, R. M. The Influence of the Surface Migration of Gold on the Growth of Silicon Nanowires. *Nature* **2006**, *440*, 69–71.
11. Bae, J.; Kulkarni, N. N.; Zhou, J. P.; Ekerdt, J. G.; Shih, C.-K. VLS Growth of Si Nanowires Using Ga and Al Catalysts. *J. Cryst. Growth* **2008**, *310*, 4407–4411.
12. Givargizov, E. I. Fundamental Aspects of VLS Growth. *J. Cryst. Growth* **1975**, *31*, 20–30.
13. Bootsma, G. A.; Gassen, H. J. A Quantitative Study on the Growth of Silicon Whiskers from Silane and Germanium Whiskers from Germane. *J. Cryst. Growth* **1971**, *10*, 223–234.
14. Sharma, S.; Kamins, T. I.; Williams, R. S. Diameter Control of Ti-Catalyzed Silicon Nanowires. *J. Cryst. Growth* **2004**, *267*, 613–618.
15. Aella, P.; Ingole, S.; Petuskey, W. T.; Picraux, S. T. Influence of Plasma Stimulation on Si Nanowire Nucleation and Orientation Dependence. *Adv. Mater.* **2007**, *19*, 2603–2607.
16. Wang, Y.; Schmidt, V.; Senz, S.; Gösele, U. Epitaxial Growth of Silicon Nanowires Using an Aluminium Catalyst. *Nat. Nanotechnol.* **2006**, *1*, 186–189.
17. Cao, L.; Garipcan, B.; Atchison, J. S.; Ni, C.; Nabet, B.; Spanier, J. E. Instability and Transport of Metal Catalyst in the Growth of Tapered Silicon Nanowires. *Nano Lett.* **2006**, *6*, 1852–1857.
18. Claassen, W. A. P.; Bloem, J. The Nucleation of CVD Silicon on SiO<sub>2</sub> and Si<sub>3</sub>N<sub>4</sub> Substrates II. The SiH<sub>2</sub>Cl<sub>2</sub>-H<sub>2</sub>-N<sub>2</sub> System. *J. Electrochem. Soc.* **1980**, *127*, 1836–1843.
19. Wagner, R. S.; Ellis, W. C. The Vapor–Liquid–Solid Mechanism of Crystal Growth and Its Application to Silicon. *Trans. Met. Soc. AIME* **1965**, *233*, 1053–1064.
20. Sirtl, E.; Hunt, L. P.; Sawyer, D. H. High Temperature Reactions in the Silicon–Hydrogen–Chlorine System. *J. Electrochem. Soc.* **1974**, *121*, 919–925.
21. Hochbaum, A. I.; Fan, R.; He, R.; Yang, P. Controlled Growth of Si Nanowire Arrays for Device Integration. *Nano Lett.* **2005**, *5*, 457–460.
22. Kayes, B. M.; Filler, M. A.; Putnam, M. C.; Kelzenberg, M. D.; Lewis, N. S.; Atwater, H. A. Growth of Vertically Aligned Si Wire Arrays Over Large Areas (>1 cm<sup>2</sup>) with Au and Cu Catalysts. *Appl. Phys. Lett.* **2007**, *91*, 103110.
23. Givargizov, E. I.; Sheftal, N. N. Morphology of Silicon Whiskers Grown by the VLS-Technique. *J. Cryst. Growth* **1971**, *9*, 326–329.
24. Garnett, E. C.; Liang, W.; Yang, P. Growth and Electrical Characteristics of Platinum-Nanoparticle-Catalyzed Silicon Nanowires. *Adv. Mater.* **2007**, *19*, 2946–2950.
25. Jeong, H.; Park, T. E.; Seong, H. K.; Kim, M.; Kim, U.; Choi, H. J. Growth Kinetics of Silicon Nanowires by Platinum Assisted Vapor–Liquid–Solid Mechanism. *Chem. Phys. Lett.* **2009**, *467*, 331–334.
26. Doerk, G. S.; Ferralis, N.; Carraro, C.; Maboudian, R. Growth of Branching Si Nanowires Seeded by Au–Si Surface Migration. *J. Mater. Chem.* **2008**, *18*, 5376–5381.
27. Kodambaka, S.; Hannon, J. B.; Tromp, R. M.; Ross, F. M. Control of Si Nanowire Growth by Oxygen. *Nano Lett.* **2006**, *6*, 1292–1296.
28. Duchemin, M. J.-P.; Bonnet, M. M.; Koelsch, M. F. Kinetics of Silicon Growth under Low Hydrogen Pressure. *J. Electrochem. Soc.* **1978**, *125*, 637–644.
29. The radial GR was also estimated directly from SEM images using  $R_{rad} = (d_b - d_i)/2t$ , where  $t$  is the growth time; both approaches yielded essentially the same results.
30. Bloem, J.; Claassen, W. A. P.; Valkenburg, W. G. J. N. Rate-Determining Reactions and Surface Species in CVD Silicon: IV. The SiCl<sub>4</sub>-H<sub>2</sub>-N<sub>2</sub> and the SiHCl<sub>3</sub>-H<sub>2</sub>-N<sub>2</sub> System. *J. Cryst. Growth* **1982**, *57*, 177–184.
31. Lew, K.-K.; Redwing, J. M. Growth Characteristics of Silicon Nanowires Synthesized by Vapor–Liquid–Solid Growth in Nanoporous Alumina Templates. *J. Cryst. Growth* **2003**, *254*, 14–22.
32. Oehler, F.; Gentile, P.; Baron, T.; Ferret, P. The Effects of HCl on Silicon Nanowire Growth: Surface Chlorination and Existence of a ‘Diffusion-Limited Minimum Diameter’. *Nanotechnology* **2009**, *20*, 475307.
33. den Hertog, M. I.; Rouviere, J. L.; Dhalluin, F.; Desré, P. J.; Gentile, P.; Ferret, P.; Oehler, F.; Baron, T. Control of Gold Surface Diffusion on Si Nanowires. *Nano Lett.* **2008**, *8*, 1544–1550.
34. Büttner, C. C.; Langner, A.; Geuss, M.; Müller, F.; Werner, P.; Gösele, U. Formation of Straight 10 nm Diameter Silicon Nanopores in Gold Decorated Silicon. *ACS Nano* **2009**, *3*, 3122–3126.
35. Ge, Sh.; Jiang, K.; Lu, X.; Chen, Ya.; Wang, R.; Fan, Sh. Orientation-Controlled Growth of Single-Crystal Silicon-Nanowire Arrays. *Adv. Mater.* **2005**, *17*, 56–61.
36. Ban, V. S. Chemical Processes in Vapor Deposition of Silicon II. Deposition from SiCl<sub>3</sub>H and SiCl<sub>4</sub>. *J. Electrochem. Soc.* **1975**, *122*, 1389–1391.
37. Sakurai, S.; Nakayama, T. Adsorption, Diffusion and Desorption of Cl Atoms on Si(111) Surfaces. *J. Cryst. Growth* **2002**, *237–239*, 212–216.
38. Shudo, K.; Kirimura, T.; Tanaka, Y.; Ishikawa, T.; Tanaka, M. Quantitative Analysis of Thermally Induced Desorption During Halogen-Etching of a Silicon (111) Surface. *Surf. Sci.* **2006**, *600*, 3147–3153.
39. Wagner, R. S. A Solid–Liquid–Vapor Etching Process. *J. Cryst. Growth* **1968**, *3–4*, 159–161.
40. Hunt, L. P.; Sirtl, E. A Thorough Thermodynamic Evaluation of the Silicon–Hydrogen–Chlorine System. *J. Electrochem. Soc.* **1972**, *119*, 1741–1745.
41. Bloem, J.; Oei, Y. S.; De Moor, H.H. C.; Hanssen, J. H. L.; Giling, L. J. Near Equilibrium Growth of Silicon by CVD I. The Si–Cl–H System. *J. Cryst. Growth* **1983**, *65*, 399–405.
42. Schmidt, V.; Senz, S.; Gösele, U. Diameter Dependence of the Growth Velocity of Silicon Nanowires Synthesized via the Vapor–Liquid–Solid Mechanism. *Phys. Rev. B* **2007**, *75*, 045335.
43. Chernov, A. A. Growth Kinetics and Capture of Impurities During Gas Phase Crystallization. *J. Cryst. Growth* **1977**, *42*, 55–76.
44. Chernov, A. A.; Rusaikin, M. P. Theoretical Analysis of Equilibrium Adsorption Layers in CVD Systems (Si–H–Cl, Ga–As–H–Cl). *J. Cryst. Growth* **1978**, *45*, 73–81.

## Tapering Control of Si Nanowires grown from SiCl<sub>4</sub> at Reduced Pressure

Sergiy Krylyuk, Albert V. Davydov, and Igor Levin

Materials Science and Engineering Laboratory, National Institute of Standards and Technology,  
Gaithersburg, Maryland 20899

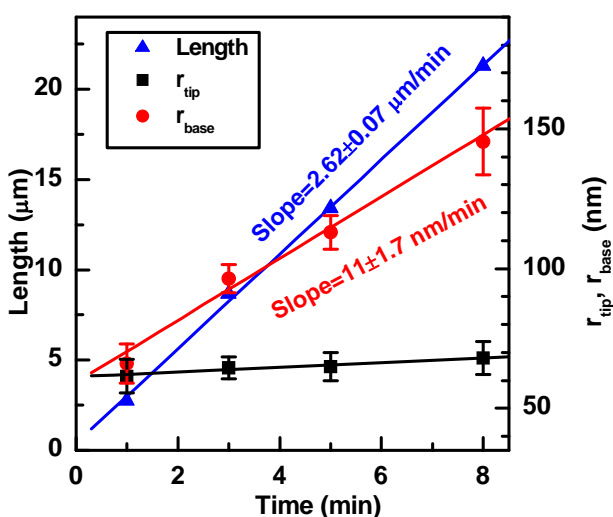


**Figure S1.** Time-evolution of tip and base radii and the length of SiNWs grown at 850 °C, 600 Torr,  $x_{\text{SiCl}_4}=0.01$  and  $\text{SiCl}_4/\text{H}_2=0.1$ . Lines are linear fits. Linear increase of the base radius with a constant tip radius indicates that tapering occurs due to Si deposition on the NW sidewalls. The slopes of the length and  $r_{\text{base}}$  dependences correspond to the vertical and lateral growth rates of 2.62  $\mu\text{m}/\text{min}$  and 11 nm/min, respectively, consistent with data for the corresponding conditions in Figure 2b.

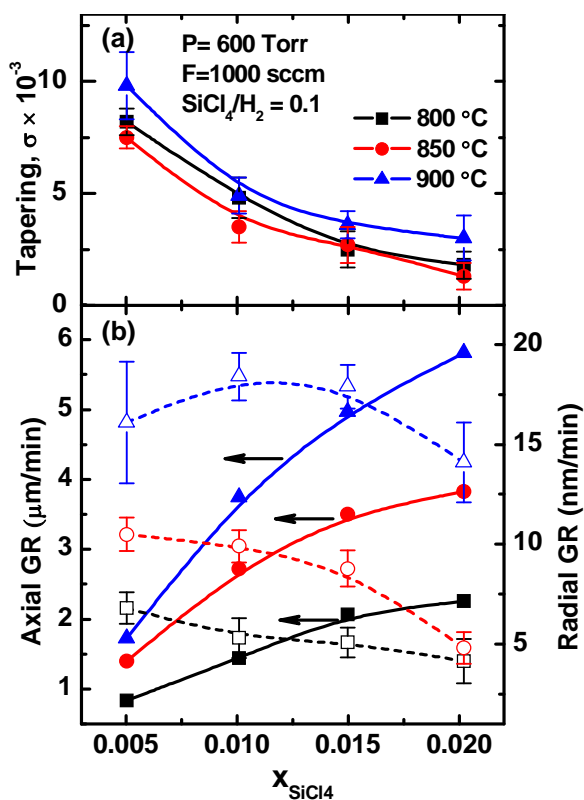


**Figure S2.** (a) Tapering factor and (b) axial (solid symbols) and radial (open symbols) growth rates as a function of SiCl<sub>4</sub> molar fraction for SiNWs grown at 800 °C, 850 °C, and 900 °C.

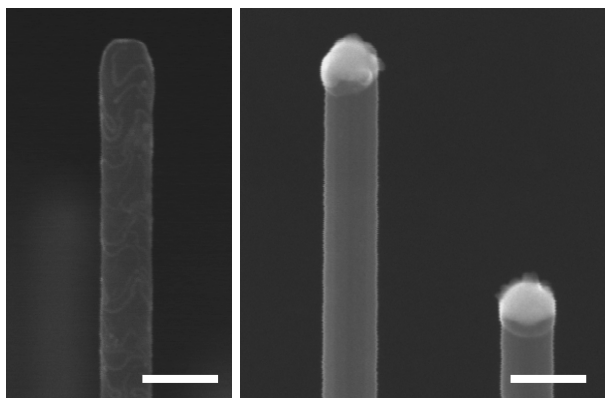


**Figure S3.** Effects of the cooling rate on post-growth Au migration out of SiNWs tips. (a) Slow cooling in nitrogen: in about 2 min to 600 °C; traces of gold are visible on the NW sidewalls. (b) Rapid cooling in nitrogen: in about 10 sec to 600 °C. The growth temperature was 850 °C. Scale bars are 200 nm.

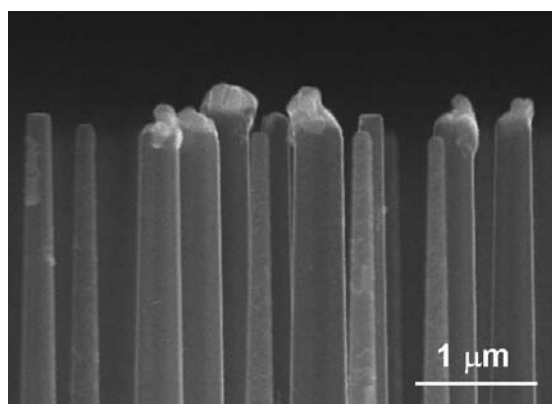


**Figure S4.** Effects of SiNW diameter on Au migration during the sample cooling (in ~3 min from 850 °C to 300 °C): for this particular experiment gold remains atop SiNWs with diameters larger *ca.* 200 nm. Note that the axial and radial GRs of SiNWs are essentially diameter-independent (i.e., taper angle is the same).

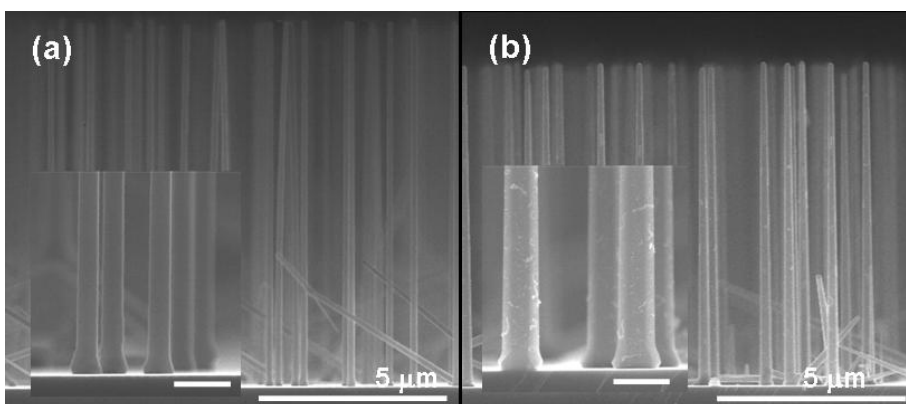


**Figure S5.** SiNWs grown at 850 °C and 600 Torr for 5 min at  $x_{\text{SiCl}_4}=0.0074$ ,  $\text{SiCl}_4/\text{H}_2=0.1$  and total gas flow rate of (a) 500 sccm and (b) 2000 sccm. Average base diameters of SiNWs are 185nm and 330 nm, respectively. Scale bars in the insets are 500 nm.

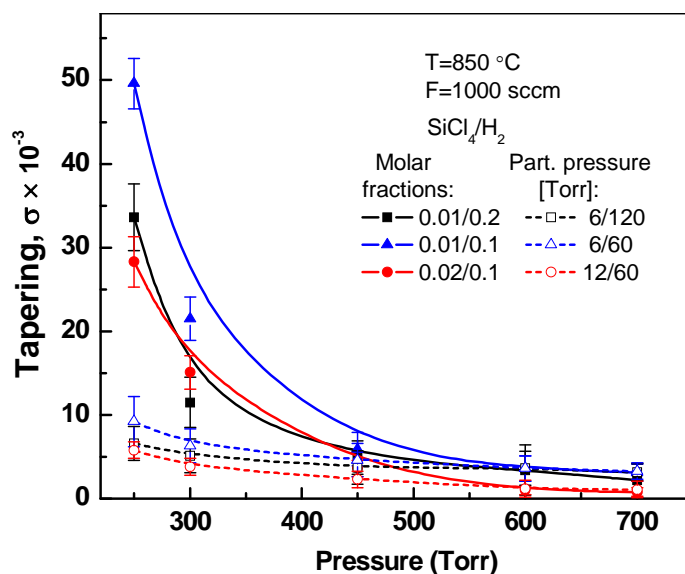


**Figure S6.** Tapering degree vs. the growth pressure for SiNWs grown at constant molar fractions (solid symbols) or at constant partial pressures (open symbols) of  $\text{SiCl}_4$  and  $\text{H}_2$ , as indicated.

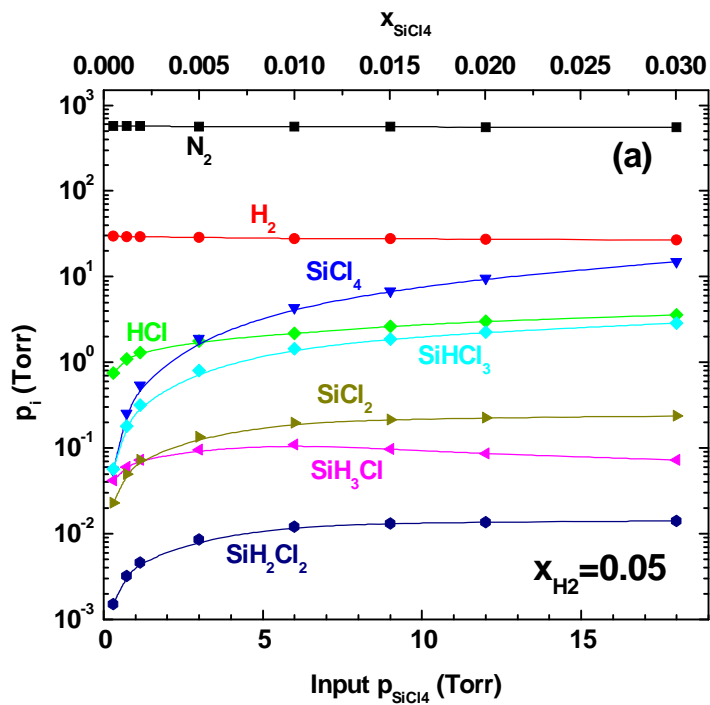


**Figure S7.** Vapor composition in the Si-Cl-H-N system calculated as a function of the input  $\text{SiCl}_4$  partial pressure for  $T=850\text{ }^\circ\text{C}$ ,  $P=600\text{ Torr}$  and hydrogen molar fraction of  $x_{\text{H}_2}=0.05$ . Corresponding input molar fractions of  $\text{SiCl}_4$  is given on the upper x-axis. Thermodynamic calculations were performed using the Thermo-Calc software and SSUB4 Substances Database. [1, 2]

[1] [www.thermocalc.com](http://www.thermocalc.com)

[2] Any mention of commercial products in this article is for information only; it does not imply recommendation or endorsement by the NIST.